Electronic Supplementary Information (ESI)

Hierarchically porous electrospun nanofibrous mats produced from intrinsically microporous fluorinated polyimide for the removal of oils and non-polar solvents

Fuat Topuz[a,] Mahmoud A. Abdulhamid,[a] Suzana P. Nunes[a,b] and Gyorgy Szekely[a,c*]*

[a]Advanced Membranes and Porous Materials Center, Physical Science and Engineering Division (PSE), King Abdullah University of Science and Technology (KAUST), Thuwal, 23955-6900, Saudi Arabia

[b] Biological and Environmental Science and Engineering, King Abdullah University of Science and Technology (KAUST), Thuwal, 23955-6900, Saudi Arabia

[c] School of Chemical Engineering and Analytical Science, University of Manchester, The Mill, Sackville Street, Manchester M1 3BB, United Kingdom

** To whom correspondence should be addressed: Dr. F. Topuz (fuat.topuz@kaust.edu.sa), Prof. G. Szekely (gyorgy.szekely@kaust.edu.sa). Phone: +966128082769.*

Table of Contents

Experimental Section S3

Characterization S3

Membrane Preparation S3

Table S1. The characteristics of the 6FDA-TrMPD polyimide. Weight (M_w) and number (M_n) average molecular weights, polydispersity index (PDI), degradation temperature $T_{d,5\%}$, and surface area (S_{BET}). S3

Fig. S1. ^{1}H NMR spectrum of the 6FDA-TrMPD in DMSO-d_6. S4

Fig. S2. Attenuated total reflectance Fourier-transform infrared spectrum (ATR-FTIR) spectrum of the 6FDA-TrMPD. S4

Fig. S3. TGA thermograms of the 6FDA-TrMPD (a) powder and (b) electrospun mat. S5

Fig. S4. The use of the electrospun mat for water-oil separation. (a) Before, and (b-d) during the separation process. S5

Fig. S5. Stress-strain curves of the free standing film made truly from the 6FDA-TrMPD powder (a) and its electrospun mat (b). S6

Fig. S6. Contact angle measurements of the fiber mat for various oils. The mat imbibed oil droplets immediately upon contact with the droplet (i.e. oil contact angle (OCA) < 1°), demonstrating superoleophilicity. S6

Fig. S7. The influence of the applied voltage on the morphology of the 6FDA-TrMPD nanofibers. $c_{6FDA\text{-}TrMPD}$= 10% (w/v). The tip-to-collector distance kept at 15 cm and the flow rate set to 0.5 mL/h. Insets show the statistical distribution for the diameter of the respective nanofibers. S7

Fig. S8. The influence of the flow rate on the morphology of the 6FDA-TrMPD nanofibers. $c_{6FDA\text{-}TrMPD}$= 10% (w/v). The applied voltage was 20 kV and the tip-to-collector distance kept at 15 cm. Insets show the statistical distribution for the diameter of the respective nanofibers. S7

Fig. S9. Scanning electron micrographs of the 6FDA-TrMPD nanofibers exposed to various solvents for 24 h. $c_{6FDA\text{-}TrMPD}$= 10% (w/v). (a) Control sample without any solvent treatment, (b) water, (c) ethanol (EtOH), (d) hexane, and (e) acetonitrile (ACN). S8

Fig. S10. Scanning electron micrographs of the electrospun mats exposed to toluene (a-c) and *m*-xylene (d-e) for 24 h. Insets show the statistical distribution for the diameter of the respective nanofibers. S8

Table S2. Oil sorption performance of various polymeric adsorbents. S9-10

Experimental Section.

Membrane Preparation. A 6FDA-TrMPD dense film was prepared through solvent evaporation from (3 wt/vol%) its polymer solution in chloroform. The solution was filtered through 0.45 μm PTFE filter and poured onto a flat glass Petri dish. The solvent was evaporated slowly at RT over 24 h. Thereafter, the obtained film was further dried at 120 °C for 24 h under vacuum. The resulting robust film with a thickness of ~ 40 μm was used for tensile measurement and for BET surface area analysis.

Characterization. The infrared spectrum was recorded for polyimide powder using a Varian 670-IR FT-IR spectrometer.

Table S1. The characteristics of the 6FDA-TrMPD polyimide. Weight (M_w) and number (M_n) average molecular weights, polydispersity index (PDI), degradation temperature $T_{d,5\%}$, and surface area (S_{BET}).

Polymer	M_w (g mol^{-1})	M_n (g mol^{-1})	PDI (-)	$T_{d,5\%}$ ($^{\circ}$C)	S_{BET} (m^2 g^{-1})
6FDA-TrMPD	176,606	110,987	1.59	509	450 ±15

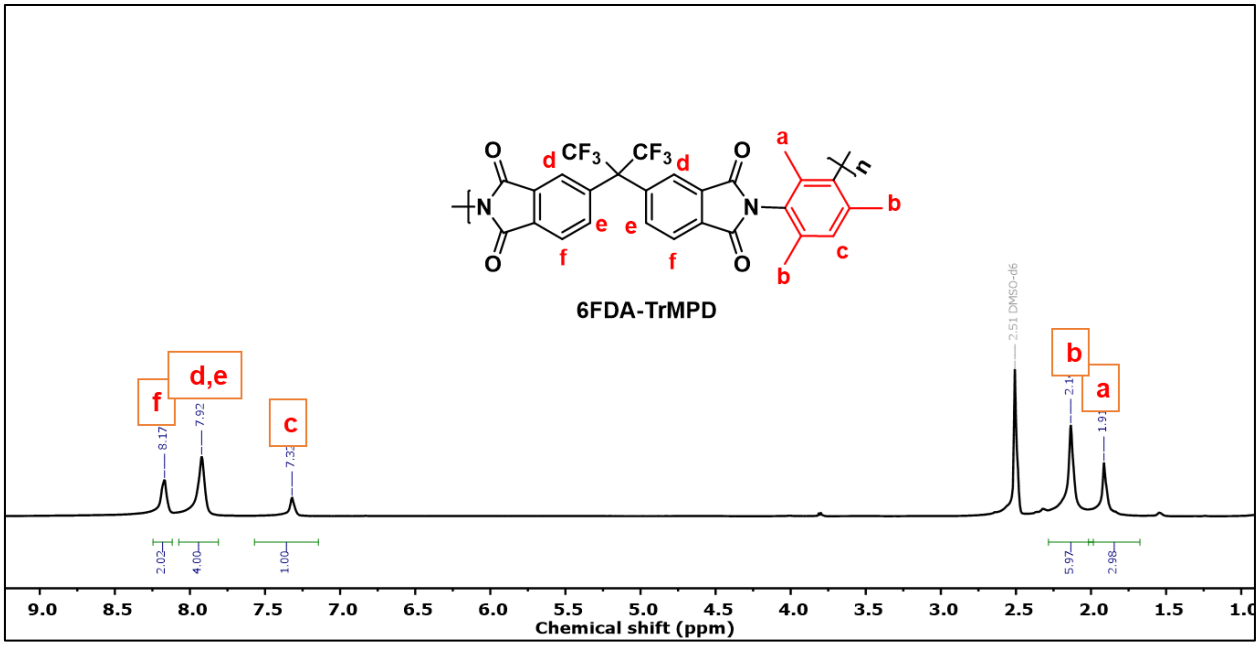

Fig. S1. ^{1}H NMR spectrum of the 6FDA-TrMPD in DMSO-d$_{6}$.

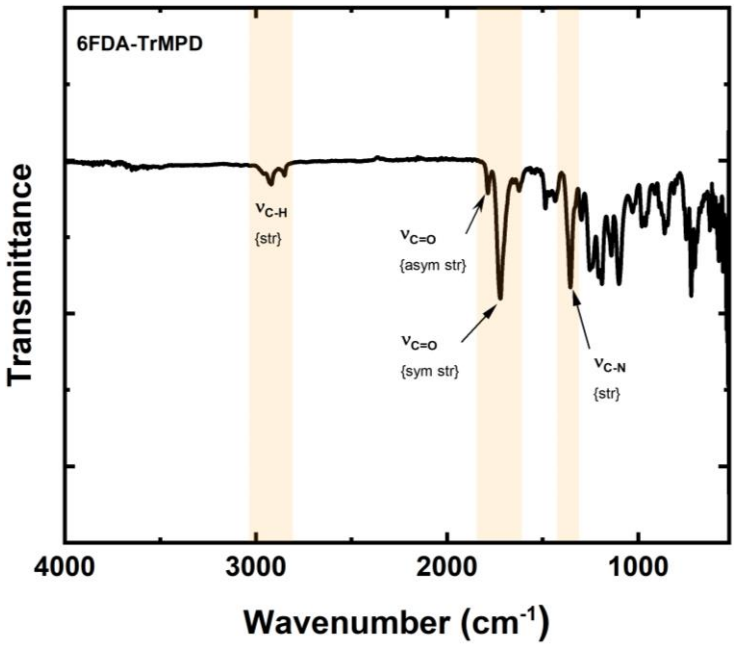

Fig. S2. Attenuated total reflectance Fourier-transform infrared spectrum (ATR-FTIR) spectrum of the 6FDA-TrMPD.

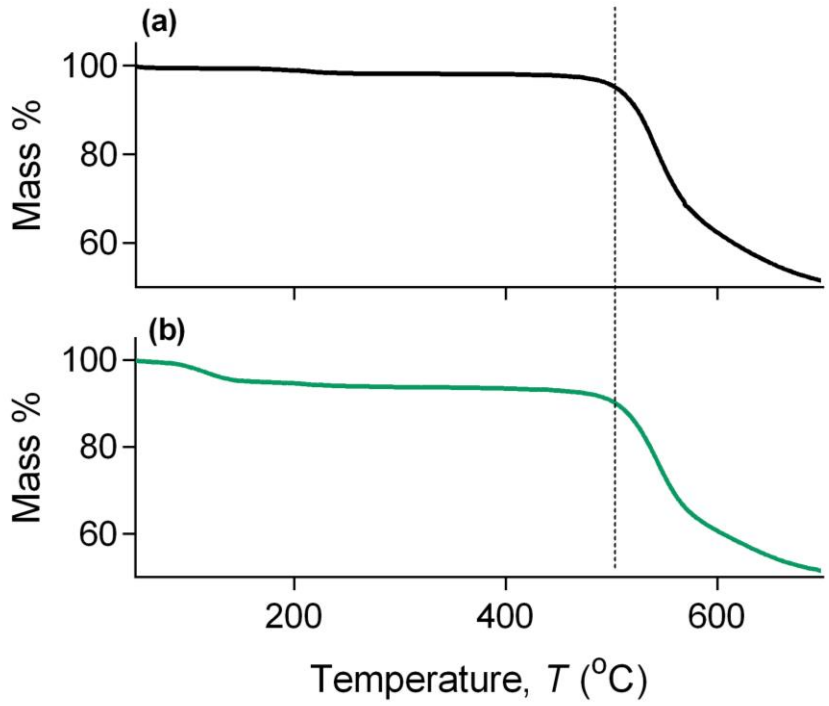

Fig. S3. TGA thermograms of the 6FDA-TrMPD (a) powder and (b) electrospun mat.

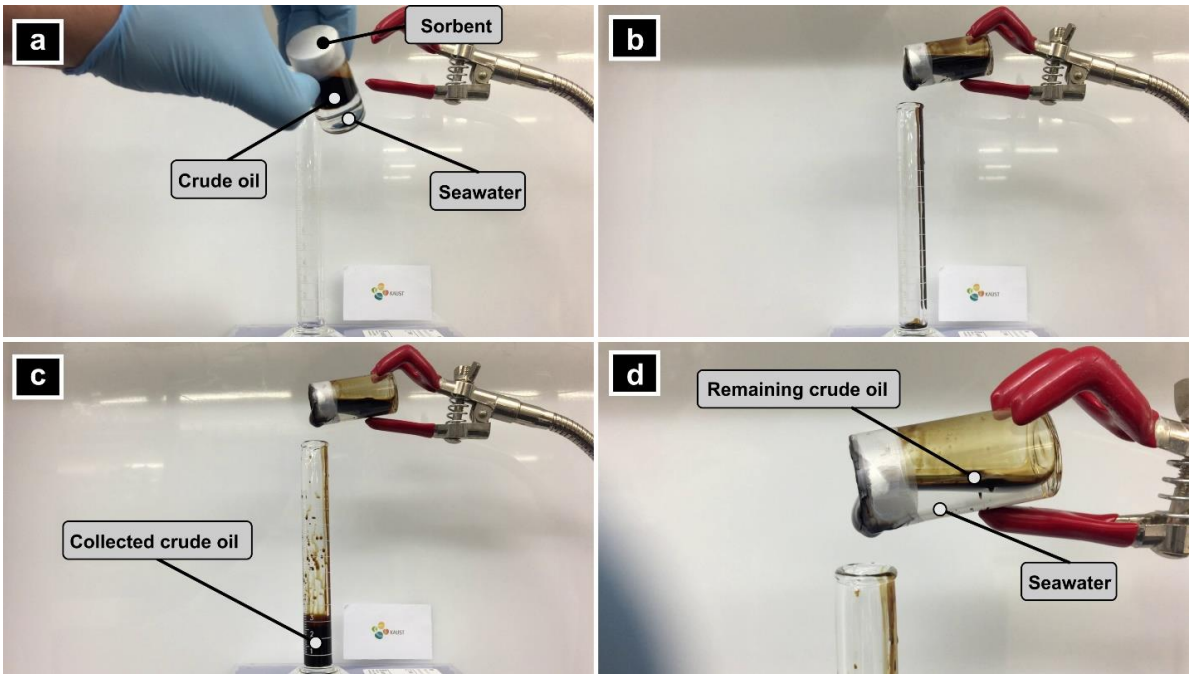

Fig. S4. The use of the electrospun mat for water-oil separation. (a) Before, and (b-d) during the separation process.

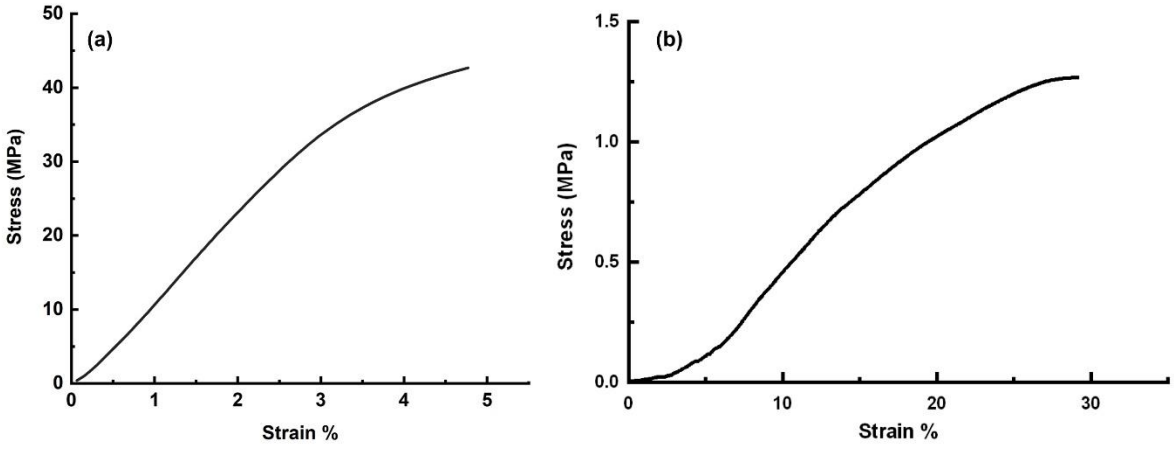

Fig. S5. Stress-strain curves of the free standing film made truly from the 6FDA-TrMPD powder (a) and its electrospun mat (b).

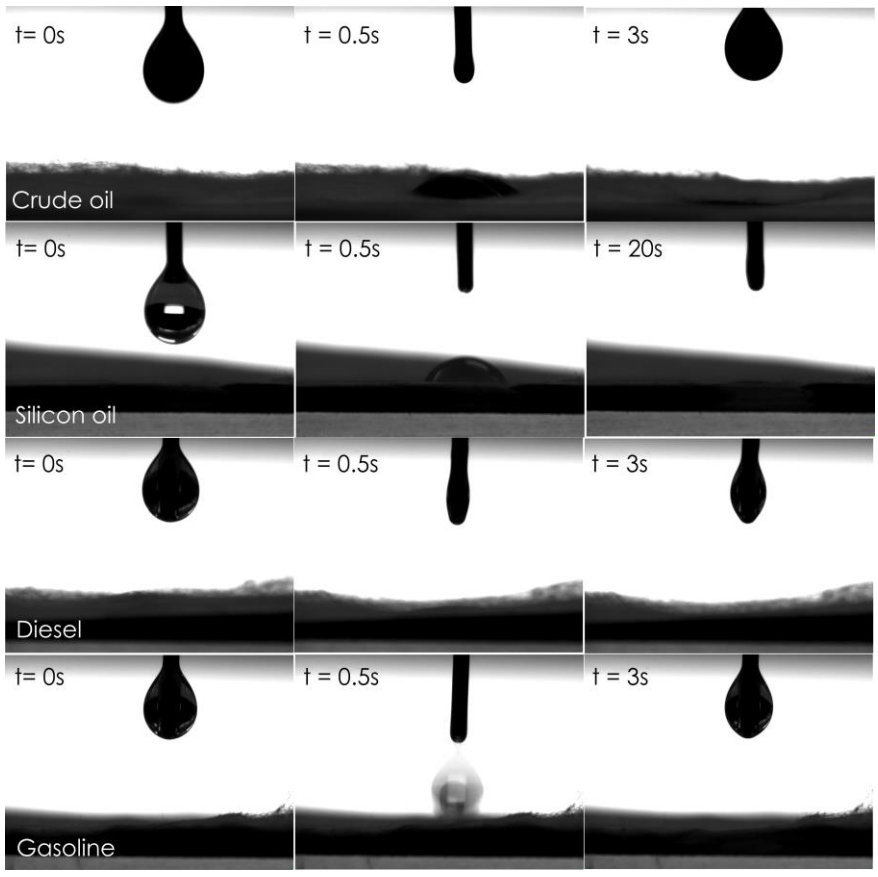

Fig. S6. Contact angle measurements of the fiber mat using various oils. The mat imbibed oil droplets immediately upon contact with the droplet (*i.e.* oil contact angle (OCA) < 1°), demonstrating superoleophilicity.

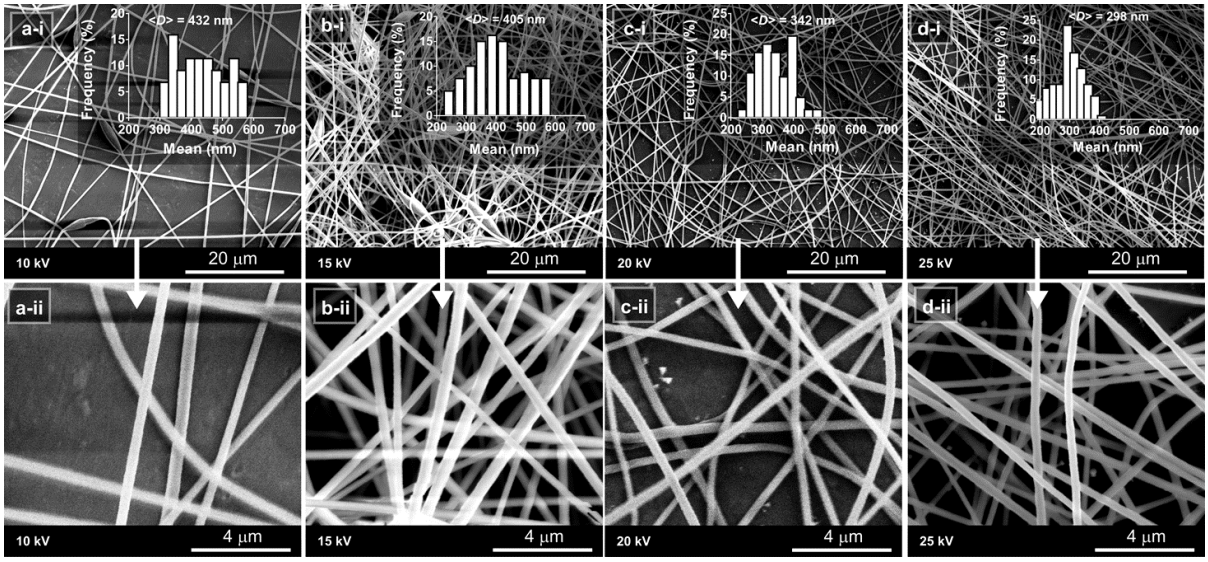

Fig. S7. The influence of the applied voltage on the morphology of the 6FDA-TrMPD nanofibers. $c_{6FDA\text{-}TrMPD}$= 10% (w/v). The tip-to-collector distance kept at 15 cm and the flow rate set to 0.5 mL/h. Insets show the statistical distribution for the diameter of the respective nanofibers.

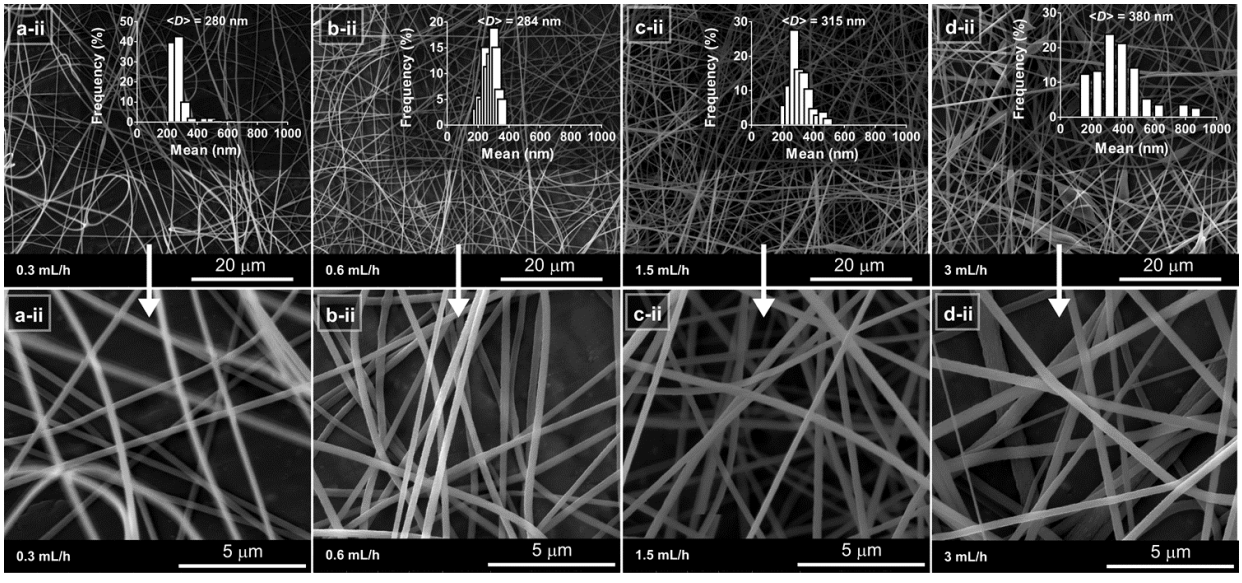

Fig. S8. The influence of the flow rate on the morphology of the 6FDA-TrMPD nanofibers. $c_{6FDA\text{-}TrMPD}$= 10% (w/v). The applied voltage was 20 kV and the tip-to-collector distance kept at 15 cm. Insets show the statistical distribution for the diameter of the respective nanofibers.

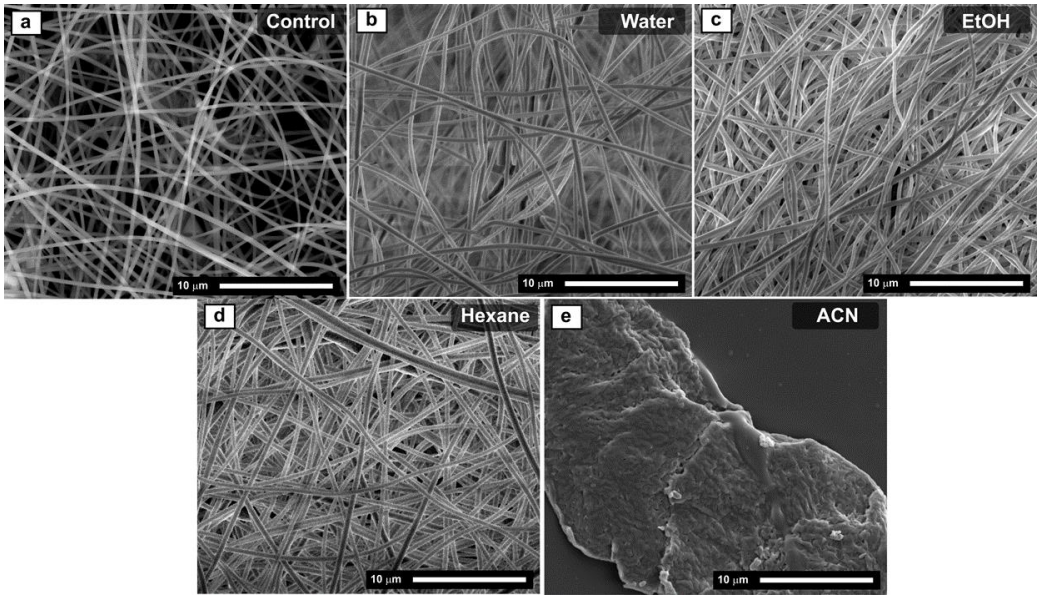

Fig. S9. Scanning electron micrographs of the 6FDA-TrMPD nanofibers exposed to various solvents for 24 h. $c_{6FDA\text{-}TrMPD}$= 10% (w/v). (a) Control sample without any solvent treatment, (b) water, (c) ethanol (EtOH), (d) hexane, and (e) acetonitrile (ACN).

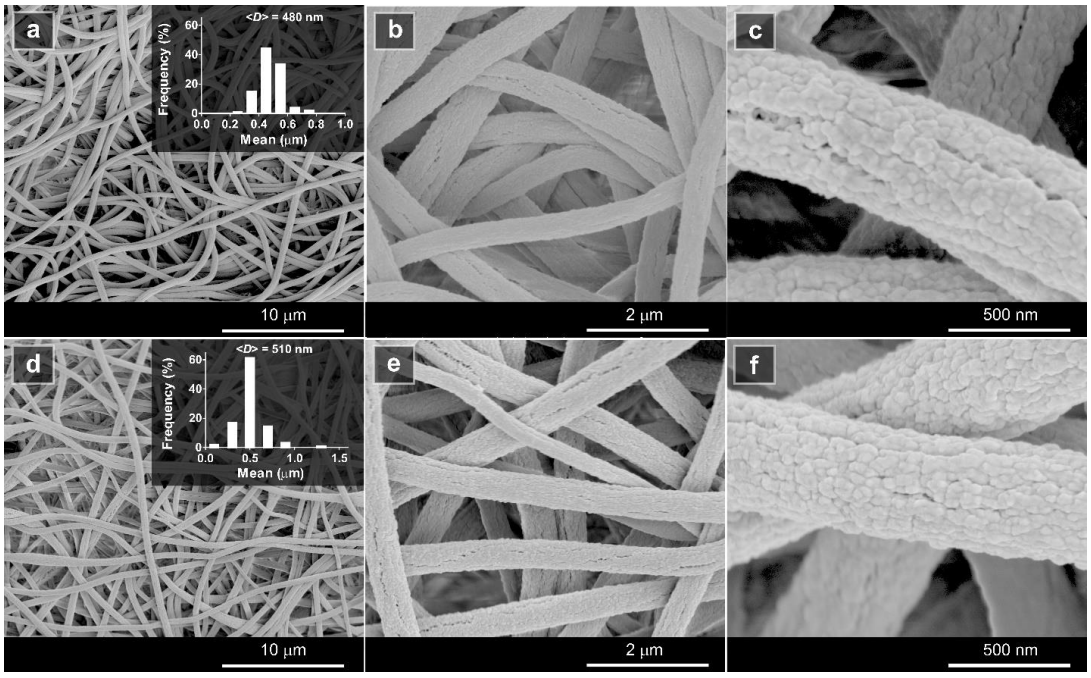

Fig. S10. Scanning electron micrographs of the electrospun mats exposed to toluene (a-c) and m-xylene (d-e) for 24 h. Insets show the statistical distribution for the diameter of the respective nanofibers.

Table S2. Oil sorption performance of various polymeric adsorbents.

Sorbent	Material form	BET surface area ($m^2 g^{-1}$)	Sorbate	Sorption capacity ($g g^{-1}$)	Ref.
Intrinsically porous fluorinated polyimides	Fibrous mat	560	Crude oil	34.6	This study
			Diesel	55.76	
			Gasoline	31.25	
A porous superhydrophobic SiO_2@polystyrene	Foam	n.d.	Crude oil	32.1	[1]
Bio-based oil gelling agent	Powder	n.d.	Crude oil	4.7	[2]
SiO_2 decorated cotton fibers	Fibers	n.d.	Crude oil	57.0	[3]
			Diesel	25.61	
Porous PS fibers	Fibers	n.d.	Diesel	7.13	[4]
Carbon shoot sponge	Sponge	440	Crude oil	~30	[5]
Cellulose-based aerogels	Aerogel	n.d.	Crude oils	18.4-20.5	[6]
Graphene sponge	Sponge	n.d.	Crude oil	85-90	[7]
CNF/carbon foam	Foam	n.d.	Diesel	21	[8]
			Gasoline	16	
Lignin-based polyurethane/graphene oxide foam	Foam	n.d.	Crude oil	25.4	[9]
Poly(dimethylsiloxane)-TiO2 coated polyurethane sponge	Sponge	n.d.	Diesel	14.2	[10]

n.d.: Not determined

References

1. C. Yu, W. Lin, J. Jiang, Z. Jing, P. Hong and Y. Li, Preparation of a porous superhydrophobic foamfrom waste plastic and its application for oil spillcleanup, *RSC Advances*, 2019, **9**, 37759-37767. https://doi.org/10.1039/C9RA06848A

2. P. Lv, S. Yang and P.-C. Ma, Bio-based oil gelling agent for effective removal of oil spills from the surface of water, *Materials Chemistry Frontiers*, 2018, **2**, 1784-1790. https://doi.org/10.1039/C8QM00127H

3. N. Lv, X. Wang, S. Peng, L. Luo and R. Zhou, Superhydrophobic/superoleophilic cotton-oilabsorbent: preparation and its application in oil/water separation, *RSC Advances*, 2018, **8**, 30257-30264. https://doi.org/10.1039/C8RA05420G

4. J. Wu, N. Wang, L. Wang, H. Dong, Y. Zhao and L. Jiang, Electrospun Porous Structure Fibrous Film with High Oil Adsorption Capacity, *ACS Applied Materials & Interfaces*, 2012, **4**, 3207-3212. https://doi.org/10.1021/am300544d

5. Y. Gao, Y. S. Zhou, W. Xiong, M. Wang, L. Fan, H. Rabiee-Golgir, L. Jiang, W. Hou, X. Huang, L. Jiang, J.-F. Silvain and Y. F. Lu, Highly Efficient and Recyclable Carbon Soot Sponge for Oil Cleanup, *ACS Applied Materials & Interfaces*, 2014, **6**, 5924-5929. https://doi.org/10.1021/am500870f

6. S. T. Nguyen, J. Feng, N. T. Le, A. T. T. Le, N. Hoang, V. B. C. Tan and H. M. Duong, Cellulose Aerogel from Paper Waste for Crude Oil Spill Cleaning, *Industrial & Engineering Chemistry Research*, 2013, **52**, 18386-18391. https://doi.org/10.1021/ie4032567

7. R.-F. Shiu, C.-L. Lee, P.-Y. Hsieh, C.-S. Chen, Y.-Y. Kang, W.-C. Chin and N.-H. Tai, Superhydrophobic graphene-based sponge as a novel sorbent for crude oil removal under various environmental conditions, *Chemosphere*, 2018, **207**, 110-117. https://doi.org/10.1016/j.chemosphere.2018.05.071

8. N. Xiao, Y. Zhou, Z. Ling and J. Qiu, Synthesis of a carbon nanofiber/carbon foam composite from coal liquefaction residue for the separation of oil and water, *Carbon*, 2013, **59**, 530-536. https://doi.org/10.1016/j.carbon.2013.03.051

9. O. Oribayo, X. Feng, G. L. Rempel and Q. Pan, Synthesis of lignin-based polyurethane/graphene oxide foam and its application as an absorbent for oil spill clean-ups and recovery, *Chemical Engineering Journal*, 2017, **323**, 191-202. https://doi.org/10.1016/j.cej.2017.04.054

10. Q. Shuai, X. Yang, Y. Luo, H. Tang, X. Luo, Y. Tan and M. Ma, A superhydrophobic poly(dimethylsiloxane)-TiO2 coated polyurethane sponge for selective absorption of oil from water, *Materials Chemistry and Physics*, 2015, **162**, 94-99. https://doi.org/10.1016/j.matchemphys.2015.05.011